Mateusz Czerwienko[1], Andrzej Uramek[1], Rafal P. Wojda[1,2]

ABB Corporate Research Center Krakow Poland (1), Electric Energy Systems Integration Group at Oak Ridge National Laboratory (2)
doi:10.15199/48.2019.06.19

Derivation of The Planar Square Coil Litz-Wire Winding Resistance for Sinusoidal Currents

Abstract. *In this paper the AC winding resistance of the litz wire wound planar square coil is derived. The Biot-Savart's law is used to derive analytical expression for the AC winding resistance. Analytical calculations are done for two planar square coils of different size. Experimental verification and comparison of the calculated and measured winding resistances are performed.*

Streszczenie. *W artykule tym, wyprowadzone zostało rownanie na rezystancję uzwojenia cewek planarnych w kształcie kwadratu przewodzących prąd przemienny. Rezystancja takich cewek nie jest stała lecz zmienia się wraz ze wzrostem czestotliwości. Przyczyną zmiany tejże rezystancji jest przede wszystkim efekt zbliżeniowy, który powstaje podczas indukowania się prądow wirowych w uzwojeniu. Wpływ efektu zbliżeniowego na rezystancje uzwojenia jest silniejszy wraz ze wzrostem czestotliwości. Analityczne równanie na rezystancję uzwojenia dla prądow przemiennych takiej cewki, wyprowadzono bazując na prawie Biot-Savart's. Experymentalna weryfikacja i porównanie teoretycznych obliczeń została również dokonana i przedstawiona w tym artykule.**(Wyprowadzenie równania na rezystancję uzwojenia planarnej cewki w kształcie kwadratu pracującej w obwodach rezonansowych z prądem sinusoidalnym)***

Keywords: AC winding resistance, eddy currents, planar square coil, proximity effect, power loss, wireless power transfer
Słowa kluczowe: Bezprzewodowy przesył energii, efekt zblizeniowy, planarna kwadratowa cewka, prądy wirowe, Rezystancja AC uzwojenia, straty mocy.

Nomenclature

$\gamma = r_s\sqrt{\mu\sigma\omega}$ - normalized radius of the strand;
δ - skin depth;
μ - free space magnetic permeability;
σ - copper conductor conductivity;
$\omega = 2\pi f$ - angular frequency of the conductor current;
ESR - equivalent series resistnace;
I - RMS value of the coil current;
N_s - number of strands in the litz wire;
N_t - number of the coil turns;
L_i, L_j - lengths of i^{th} and j^{th} coil sides;
P_j - the power dissipated in the conductor j-th turn (one side of the coil);
R_{coil} - total resistance of the coil;
$R_{dc},\ R_{dcm}$ - calculated and measured copper solid round wire DC resistance;
R_{meas} - measured AC winding resistance;
$R_{prox},\ R_{proxm}$ - calculated and measured proximity effect winding resistance of the coil winding;
R_{skin} - skin effect winding resistance of the litz wire;
$i_l(t)$ - sinusoidal winding conductor current;
$f,\ f_{critical}$ - operating frequency and critical frequency;
i - index of the conductor turn for which magnetic field intensity is calculated - victim;
j - index of the conductor turn which conducts alternating current - attacker;
r_c - radius of the conductor bundle;
l - the length of the winding conductor;
r_s - one strand radius;
$v_e(t)$ - sinusoidal voltage induced on the conductor surface.

Introduction

Demand of the wireless power transfer systems (WPT) for the high quality factor planar coils is significantly increasing. It can be seen that planar coils are utilized in systems like inductive heating, EV charging, robot charging, home appliances, medical appliances, and mobile device systems [20]-[36]. The addition of the ferrite introduces ferrite core losses and increases copper losses [19]. The air-core inductor with advantages of even magnetic field distribution and relatively lower costs could be utilized in such a systems [20]. Moreover in all of these systems, the low-loss planar inductors are required in order to increase the quality factor and to transfer energy with the highest possible efficiency. The WPT coils operate at relatively low coupling factor (typical range 0.1 to 0.4), thus, there is a presence of high circulating currents that causes additional copper losses. These losses must be reduced in order to increase the WPT system efficiency thus high unloaded quality factor coils are required.

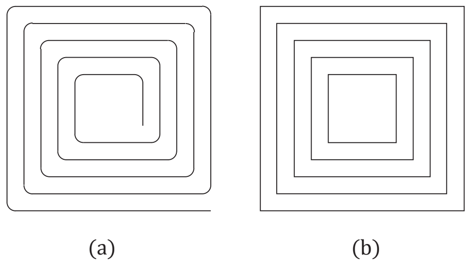

Fig. 1. The planar square air-core coil. (a) The planar square air-core coil. (b) The simplified planar square air-core model.

Utilization of the litz-wire windings in the air-core planar inductors assures that the high-frequency winding resistance is relatively low, and therefore, high total efficiency of the WPT system is easily achieved. This is mainly because the litz-wire conductors are braided from many insulated thin strands that prevent eddy-currents induction.

The high-frequency losses of the planar air-core inductors wound with the litz-wire winding are caused by two orthogonal eddy current effects, the skin effect and the proximity effect. The skin effect is caused by the applied alternating current $i_l(t)$ in the conductor. This current induces time-varying magnetic flux $\phi_\alpha(t)$ and from Faraday's law time-varying voltage $v_e(t)$ is induced on conductor surface. From the Lenz's law, the direction of the voltage $v_e(t)$ is such that it induced current $i_e(t)$, which in turn induces magnetic flux $\phi_\beta(t)$ that oppose change in the applied flux $\phi_\alpha(t)$. As a result, the applied alternating current $i_l(t)$ is forced out from the center of the conductor to its surface.

For the proximity effect, the alternating current $i_l(t)$ in the conductor induces the time-varying voltage $v_e(t)$ on the surface of the adjacent conductors. The induced voltage $v_e(t)$ from the Faraday's law induces the eddy currents in these conductors, altering current density distribution in the conductor's cross section, so the applied current tends to flow in the conductor surface.

Thus, the current density distribution in the adjacent conductors depends of the direction and frequency of the applied current $i_l(t)$. For the same current direction, the current density distributes to the outer surface of adjacent conductors what is called the proximity effect. For the opposite current direction, the current density distributes to the inner surface of adjacent conductors what is called the anti-proximity effect [14]. As the frequency increases, the magnitude of the eddy current increases, and therefore, applied current tends to flow closer to the conductor surface. The total eddy current density J_e is the superimposition of the skin and proximity effects current densities $J_e = J_{skin} + J_{prox}$. Orthogonality of skin and proximity effects imposes that their resistances could be separately studied [1]-[11], [14]-[16].

For the winding resistance calculation both the analytical and the numerical methods are used. The big advantage of the analytical methods is that it outweigh FEM method in terms of computational effort. For the small number of strands in the litz wire bundle, there is possibility to calculate the winding resistance using FEM in reasonable time. However, for the large number of strands $n_0 > 10$, FEM calculations takes up to few days, while analytic methods takes no time.

Various analytic methods are used for the litz-wire winding resistance calculation [1]-[13], [18]-[22], [26], [28]. In these papers one-dimensional model is used for derivation of the winding resistances based on Maxwell's equation (Ampere's law) and Biot-Savart's law.

In this paper, the Biot-Savart's law is used to derive the average magnetic field induced in the litz wire conductor cross section for the planar square air-core coil. Objectives of this study are:

- Introduction of the planar square air-core coil model;
- Derivation of the proximity effect winding resistance of the planar square air-core coil;
- Comparison of the calculated and measured winding resistances for two planar square air-core coils in frequency range 0 to 500 kHz.

Model of The Planar Square Air-Core Coil

Fig. 1 shows the planar square air-core coil. Note that corners of the coil in Fig. 1a are bent. For simplification of the winding loss calculation, the planar coil corners are assumed to be at right angles as in Fig. 1b. The winding losses caused by a ESR of the litz-wire air coil consist of DC and AC losses. The DC loss is the sum of losses in each copper strand of the litz wire bundle and depend of the conductor resistivity. The AC losses are the sum of the eddy current skin and proximity losses and are frequency dependent. The self-induced eddy currents loss for higher frequencies far exceeds the DC loss.

Because of the skin and proximity effects orthogonality the ESR of the coil for the sinusoidal currents is given by

$$R_{coil}(f) = R_{skin}(f) + R_{prox}(f), \tag{1}$$

where the low and medium frequency skin effect winding resistance is given by [2], [14]

$$R_{skin}(f) \approx R_{dc}F_R(f) \approx R_{dc}\left[1 + \frac{1}{48}\left(\frac{r_s}{\delta}\right)^4\right]. \tag{2}$$

For $r_s \ll \delta/\sqrt{2}$ the skin effect winding resistance can be neglected, determining critical frequency $f_{critical}$ as

$$r_s \ll \frac{1}{\sqrt{\omega\mu\sigma}} \quad \Rightarrow \quad f \ll \frac{1}{2\pi\mu\sigma r_s^2}, \tag{3}$$

TABLE I: COPPER LITZ WIRE PARAMETERS

Number of strands n_0	Strand radius r_s (mm)	Bundle radius r_c (mm)
1800	0.035	1.75

TABLE II: COIL PARAMETERS

Coil number	Turns number	Internal width (mm)	External width (mm)
1	13	155	260
2	25	60	260

$$f_{critical} = \frac{1}{2\pi\mu\sigma r_s^2}. \tag{4}$$

Table I lists properties of the litz-wire winding considered in this paper. For the $r_s = 35$ μm the critical frequency is $f_{critical} = 1.78$ MHz, and the skin depth of the measured litz wire at the operating frequency $f = 500$ kHz is $\delta = 93.5$ μm therefore, the skin effect can be neglected in the copper strand. Taking into account aforementioned simplifications and assumptions the simplified series resistance of the coil is

$$R_{coil}(f) = R_{dc} + R_{prox}(f) \quad \text{for } f \ll f_{critical}. \tag{5}$$

For the given geometry, the DC winding resistance is

$$R_{dc} = \frac{l}{\pi r_s^2 N_s \sigma} = \sum_{j=1}^{N_t} \frac{8(w + s(j-1))}{\pi r_s^2 N_s \sigma}. \tag{6}$$

The coil consist of N_t square-shaped turns, where each conductor turn can be both, the victim i, i.e., conductor in which the eddy currents are induced, or the attacker j, conductor that induces the eddy currents through the induced magnetic field intensity. In Figs. 2 and 3 the top view and the cross section of the planar coils are shown.

Lengths of i^{th} and j^{th} coil sides are

$$L_i = 2(w + s(i-1)), \tag{7}$$

and

$$L_j = 2(w + s(j-1)), \tag{8}$$

respectively. Lengths L_i and L_j are the integration boundaries for the winding power loss calculation.

The proximity effect winding resistance of the planar square air coil is given by [2]

$$R_{prox} = 4\sum_{j=1}^{N_t} \frac{2N_0^2 P_j}{I^2}\frac{1}{N_0}. \tag{9}$$

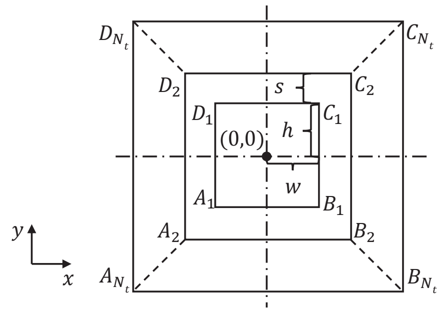

Fig. 2. Top view of the square coil.

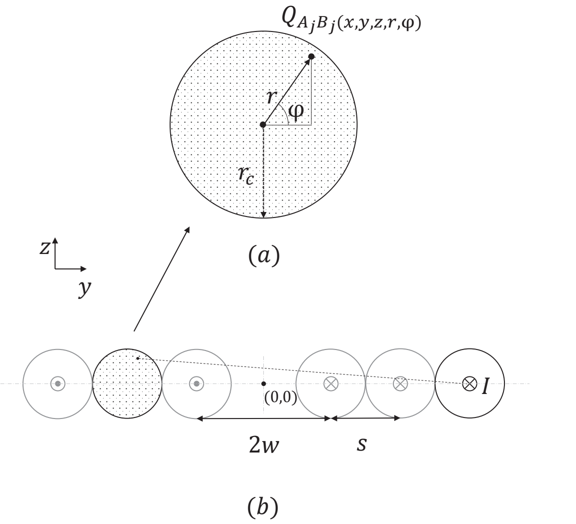

Fig. 3. Cross section of the planar coil conductors. (a) Cross section of the strand. (b) The cross section of the coil.

where P_j is

$$P_j = \int_{-L_j/2}^{L_j/2} \frac{\pi\gamma^4 H_{j,x}^2}{8\sigma}, \tag{10}$$

$\gamma = r_s\sqrt{\mu\sigma\omega} = \sqrt{2}r_s/\delta$ is the normalized radius of the strand, and $\omega = 2\pi f$ is the angular frequency of the winding current.

The averaged squared magnetic field intensity in the strand cross section $H_{j,x}^2$ is proportional to the integral of the squared magnetic field intensity at the point $Q_{A_jB_j(x,y,z,r,\varphi)}$ (Fig. 3), with respect to r and φ and inversely proportional to the strand cross-sectional area

$$H_{j,x}^2 = \frac{1}{\pi r_c^2}\int_0^{r_c}\int_0^{2\pi} H_{j,(x,r,\varphi)}^2 d\varphi dr. \tag{11}$$

The influence of the *z* and *y* components of the magnetic field intensity on the effective magnetic field intensity $H_{j(x,r,\varphi)}^2$ are twice that of the *x* component [2]

$$H_{j(x,r,\varphi)}^2 = H_{j,(x,r,\varphi)\_z}^2 + H_{j,(x,r,\varphi)\_y}^2 + \frac{H_{j,(x,r,\varphi)\_x}^2}{2}. \tag{12}$$

Components $H_{j,(x,r,\varphi)\_x}$, $H_{j,(x,r,\varphi)\_y}$ and $H_{j,(x,r,\varphi)\_z}$ are the sum of the magnetic fields intensities at the point $Q_{A_jB_j(x,y,z,r,\varphi)}$ caused by the ith turn of the coil (Appendix A) and are given by

(13)

$$H_{j(x,r,\varphi)\_x} = \sum_{i=1}^{N_t}(H_{BC\_i\_j(x,r,\varphi)_x} + H_{DA\_i\_j(x,r,\varphi)_x}),$$

(14)

$$H_{j(x,r,\varphi)\_y} = \sum_{i=1}^{N_t}(H_{AB\_i\_j(x,r,\varphi)_y} + H_{CD\_i\_j(x,r,\varphi)_y}),$$

and

(15)

$$H_{j(x,r,\varphi)\_z} = \sum_{i=1}^{N_t}(H_{AB\_i\_j(x,r,\varphi)_y} + H_{BC\_i\_j(x,r,\varphi)_x} + H_{DA\_i\_j(x,r,\varphi)_x} + H_{CD\_i\_j(x,r,\varphi)_y}),$$

TABLE III: MEASURED AND CALCULATED DC RESISTANCE

Coil number	Calculated (mΩ)	Measured (mΩ)
1	27	28
2	43	41

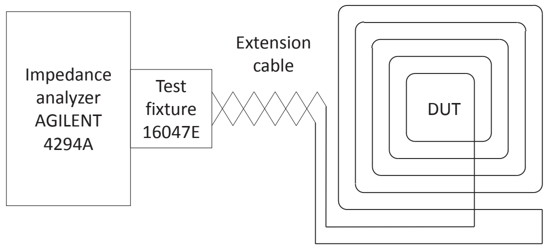

Fig. 4. The measurement setup.

respectively. Thus substituting (10), (13), (14), (15), and (12) into (9), one obtains the proximity effect winding resistance of the planar square air-core coil

$$R_{prox} = \frac{n_0\pi\gamma^4 \int_{-L_j/2}^{L_j/2} \left(\sum_{j=1}^{N_t} H_{j,x}^2\right) dx}{\sigma I^2}. \tag{16}$$

Experimental Verification

The measurement setup shown in Fig. 4 consist of:

- planar square air-core coil (Fig. 5),
- four meter extension litz wire cable,
- the Agilent 4294A impedance analyzer with the 16047E test fixture.

In order to minimize the influence of the external magnetic field intensity the external cable was twisted, and the coil was placed two meters away from the metallic objects on the non-conductive pedestal. Measurement of the DC winding resistance R_{dcm}, the AC resistance of the extension cable R_{ext}, combined coil with extension cable resistance R_{meas} have been performed, and then measured proximity effect winding resistance of the coil winding R_{prox_m} calculated

$$R_{prox\_m} = R_{meas} - R_{ext} - R_{dc\_m}. \tag{17}$$

Two coils listed in Table were measured in compliance with described method. The DC winding resistance R_{dc_m} for both cases was measured by four terminal method and listed in the Table . Extension cable was fixed to a position used for measuring the coils and resistance R_{ext} was measured with impedance analyzer, which results are shown in the Fig. 6.

Calculated R_{prox} and measured R_{prox_m} proximity effect resistance of both coils are shown in the Fig. 7 and Fig. 8.

It could be observed that for frequencies above 350 kHz for the coil No. 1 and 300 kHz for the coil No. 2 criteria from (3) incrementally ceases and underestimation of (16) occurs due to skin effect. Calculated proximity resistance captures measured winding resistance in the range of 75 kHz to 400 kHz with high accuracy. Discrepancies between measured and calculated proximity effect winding resistances for frequencies below 75 kHz are due to the fact that the impedance analyzer is not able to measure resistances below 30 mΩ.

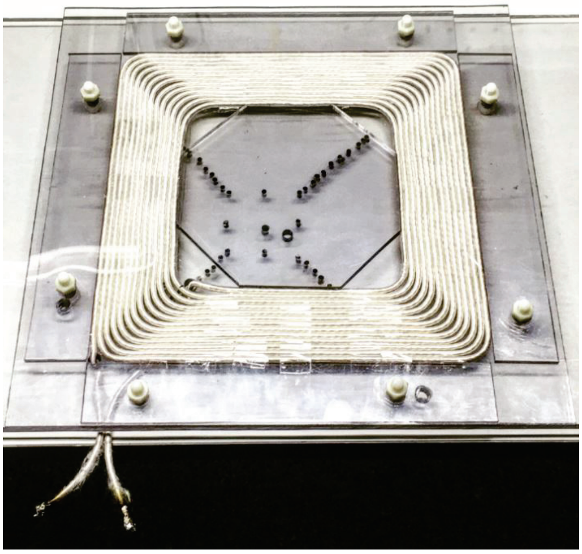

Fig. 5. Coil 2 prototype.

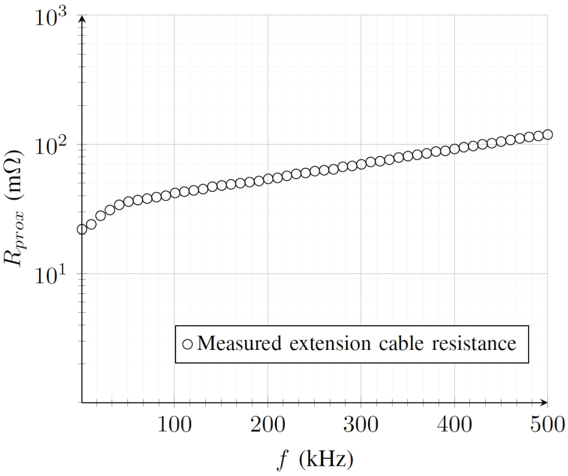

Fig. 6. The measured resistance of extension cable.

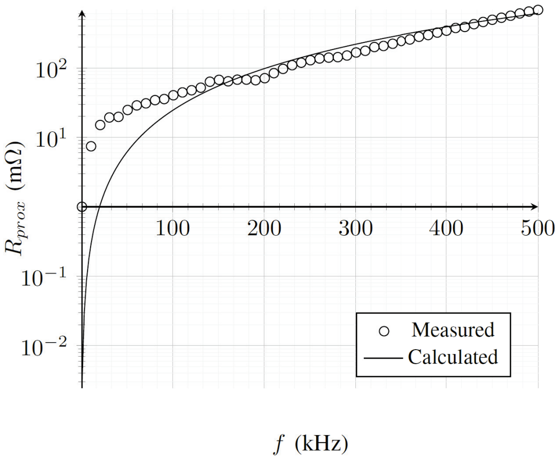

Fig. 7. The measured and calculated proximity effect winding resistance as functions of frequency for the coil no. 1.

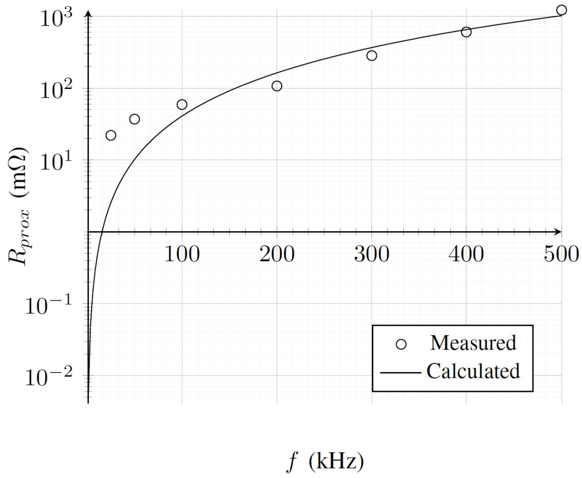

Fig. 8. The measured and calculated proximity effect winding resistance as functions of frequency for the coil no. 2.

Conclusions

Analytical method, based on Biot-Savart law, to derive the proximity-effect resistance for the square planar coil was introduced. Proposed method was used to calculate resistance of two exemplary coils designed for wireless power transfer in frequency range up to $f \ll f_{critical}$. Measurements results show that for exemplary coils, proximity effect is a major contributor to the coil total winding resistance (for $f \ll f_{critical}$). Derived formula takes into account number of turns and strands, separation between turns, strand diameter, and conductor bundle diameter as input parameters, so it can be utilized for multi-dimensional optimization of wireless power transfer coil design. Time of calculation of the resistance for exemplary coils is in order of minutes, so it is well suited for design purposes.

Experimental verification of the analyctical derivation of the proximity effect winding resistance of the square planar air core was performed. Results showed that the predicted resistances agreed with the measured ones.

REFERENCES

[1] P. L. Dowell, "Effects of eddy currents in transformer winding," *Proc. IEE*, vol. 113, no. 8, pp. 1387-1394, Aug. 1966.
[2] Q. Deng et al., "Frequency-dependent resistance of litz-wire square solenoid coils and quality factor optimization for wireless power transfer" *IEEE Transactions on Industrial Electronics,* vol. 63, no. 5, pp. 2825-2837, May 2016.
[3] G. W. O. Howe, "The high-frequency resistance of multiply-stranded insulated wire," *Proc. Royal Soc. Lon.* A, vol. 93, pp. 468-492, September 1917.
[4] M. Bartoli, N. Noferi, A. Reatti, and M. K. Kazimierczuk, "Modeling litz-wire winding losses in high-frequencies power inductors, " *Proceedings of the IEEE Power Electronics Specialists Conference*, Baveno, Italy, June 24-27, 1996. pp. 1960-1966.
[5] P. N. Murgatroyd, "Calculation of proximity losses in multi-stranded conductor branches," *IEE Proceedings,* Part A, vol. 136, no. 3, pp. 115-120, May 1989.
[6] J. A. Ferreira, "Analytical computation of AC resistance of round and rectangular litz-wire windings," *IEE Proceedings, Part B, Electric Power Applications,* vol. 139, no 1, pp. 21-25, Jan. 1992.
[7] A. W. Lotfi and F. C. Lee, "A high frequency model for litz wire for switch-mode magnetics," Proc. of the 1993 *IEEE Industry Applications Society Annual Meeting*, vol. 2, pp. 1169-1175, 1993.
[8] J. Schutz, J. Roudet, and A. Schellmanns, "Modeling litz-wire windings," *Proc. IEEE Industry Appl. Soc. Annual Meeting (IAS)*, New Orleans, LA, vol. 2, pp. 1190-1195, October 5-9, 1997.
[9] F. Tourkhani and P. Viarouge, "Accurate analytical model of winding losses in round litz-wire windings," *IEEE Tran. Magn.*, vol. 37, no. 1, pp. 538–543, Jan. 2001.

[10] J. Acero, P. J. Hernandez, J. M. Burdio, R. Alonso and L. A. Barragdan, "Simple resistance calculation in litz-wire planar windings for induction cooking appliances," *IEEE Transactions on Magnetics*, vol. 41, no. 4, pp. 1280-1288, April 2005.
[11] Acero, J., Burdio, J.M., Alonso, R., Barragan, L.A., Puyal, D.: "Frequency-dependent resistance in litz-wire planar windings for domestic induction heating appliances," *IEEE Trans. Pow. Electron.*, 21, (4), pp. 856–866, 2006.
[12] A. Rosskopf, E. Bar, and C. Joffe, "Influence of inner skin- and proximity effects on conduction in litz wires," *IEEE Tran. Pow. Electron.*, vol. 29, no. 10, pp. 5454–5461, Oct. 2006.
[13] H. Rossmanith, M. Doebroenti, M. Albach, and D. Exner, "Measurement and characterization of high frequency losses in non-ideal litz wires," *IEEE Tran. Pow. Electron.*, vol. 26, no. 11, pp. 3386–3394, Nov. 2011.
[14] M. K. Kazimierczuk, *High-Frequency Magnetic Components* 2nd Ed. John Wiley & Sons, Chichester, UK, 2012.
[15] R. P. Wojda and M. K. Kazimierczuk, "Winding resistance of litz-wire and multi-strand inductors," *IET Power Electronics*, vol. 5, no. 2, pp. 257-268, Feb. 2012.
[16] R. P. Wojda and M. K. Kazimierczuk, "Analytical optimization of solid-round-wire windings," *IEEE Transactions on Industrial Electronics*, vol. 60, no. 3, pp. 1033-1041, March 2013.
[17] R. P. Wojda and M. K. Kazimierczuk, "Winding resistance and power loss of inductors with litz and solid-round wires," *IEEE Transactions on Industry Applications*, vol. 54, no. 4, pp. 3548-3557, July 2018.
[18] R. P. Wojda and M. K. Kazimierczuk, "Analytical winding size optimisation for different conductor shapes using Ampère's Law," *IEET Power Electron.*, vol. 6, no. 6, pp. 1058-1068, June 2013.
[19] R. Bosshard, "Multi-Objective Optimization of Inductive Power Transfer Systems for EV Charging", Ph.D. dissertation, ETH Zurich, 2015.
[20] Kai Song, Kim Ean Koh, Chunbo Zhu, Jinhai Jiang, Chao Wang and Xiaoliang Huang, "A Review of Dynamic Wireless Power Transfer for In-Motion Electric Vehicles, Wireless Power Transfer - Fundamentals and Technologies", *Wireless power transfer - fundamentals and technologies,* 2016.
[21] G. A. Covic and J. T. Boys, "Modern Trends in Inductive Power Transfer for Transportation Applications," *IEEE Journal of Emerging and Selected Topics in Power Electronics,* vol. 1, no. 1, pp. 28-41, March 2013.
[22] Yang Li et al., "Wireless energy transfer system based on high Q flexible planar-Litz MEMS coils," *The 8th Annual IEEE International Conference on Nano/Micro Engineered and Molecular Systems,* pp. 837-840, Suzhou, 2013.
[23] J. Zhang, G. Song, Y. Li, G. Qiao and Z. Li, "Battery swapping and wireless charging for a home robot system with remote human assistance,"*IEEE Transactions on Consumer Electronics*, vol. 59, no. 4, pp. 747-755, November 2013.
[24] C. Qiu, K. T. Chau, C. Liu and C. C. Chan, "Overview of wireless power transfer for electric vehicle charging," *2013 World Electric Vehicle Symposium and Exhibition (EVS27),* pp. 1-9, Barcelona, 2013.
[25] M. Bojarski, E. Asa and D. Czarkowski, "Effect of wireless power link load resistance on the efficiency of the energy transfer," *2014 IEEE International Electric Vehicle Conference (IEVC),* Florence, 2014, pp. 1-7.
[26] S. Y. R. Hui, W. Zhong and C. K. Lee, "A Critical Review of Recent Progress in Mid-Range Wireless Power Transfer," *IEEE Transactions on Power Electronics,* vol. 29, no. 9, pp. 4500-4511, Sept. 2014.
[27] E. Asa, K. Colak, D. Czarkowski and B. Tamyurek, "Efficiency analysis of a bi-directional DC/DC converter for wireless energy transfer applications," *2015 IEEE Energy Conversion Congress and Exposition (ECCE),* Montreal, QC, pp. 594-598, 2015.
[28] S. Li and C. C. Mi, "Wireless Power Transfer for Electric Vehicle Applications," *IEEE Journal of Emerging and Selected Topics in Power Electronics,* vol. 3, no. 1, pp. 4-17, March 2015.
[29] X. Lu, P. Wang, D. Niyato, D. I. Kim and Z. Han, "Wireless charging technologies: fundamentals, standards, and network applications," in *IEEE Communications Surveys and Tutorials,* vol. 18, no. 2, pp. 1413-1452, Q2 2016.
[30] M. Debbou and F. Colet, "Inductive wireless power transfer for electric vehicle dynamic charging," *2016 IEEE PELS Workshop on Emerging Technologies: Wireless Power Transfer (WoW),* pp. 118-122, Knoxville, TN, 2016.
[31] R. Bosshard and J. W. Kolar, "Inductive power transfer for electric vehicle charging: Technical challenges and tradeoffs," *IEEE Power Electronics Magazine*, vol. 3, no. 3, pp. 22-30, Sept. 2016.
[32] T. Chunsen, D. Pengqi, W. Zhihui, H. Yongcan and D. Lin, "Parameter optimization method for the wireless charging system of mowing robot," *2017 IEEE PELS Workshop on Emerging Technologies: Wireless Power Transfer (WoW),* pp. 106-110, Chongqing, 2017.
[33] Z. Luo and X. Wei, "Analysis of square and circular planar spiral coils in wireless power transfer system for electric vehicles," *IEEE Transactions on Industrial Electronics*, vol. PP, no. 99, pp. 1-1., 2017.
[34] "Wireless power transfer for light-duty plug-in/ electric vehicles and alignment methodology," SAE J2954, Rev. May 2016.
[35] https://www.qualcomm.com/products/halo
[36] https://www.pluglesspower.com/